## Tunable Kondo effect in a bilayer graphene quantum channel

Josep Ingla-Aynés,<sup>1,\*</sup> Serhii Volosheniuk,<sup>1</sup> Talieh S. Ghiasi,<sup>1</sup> Angelika Knothe,<sup>2</sup> Kenji Watanabe,<sup>3</sup> Takashi Taniguchi,<sup>4</sup> Vladimir I. Fal'ko,<sup>5,6</sup> and Herre S. J. van der Zant<sup>1</sup>

<sup>1</sup>Kavli Institute of Nanoscience, Delft University of Technology, Lorentzweg 1, 2628 CJ Delft, The Netherlands

<sup>2</sup>Institut für Theoretische Physik, Universität Regensburg, D-93040 Regensburg, Germany

<sup>3</sup>Research Center for Functional Materials, National Institute for Materials Science, 1-1 Namiki, Tsukuba 305-0044, Japan

<sup>4</sup>International Center for Materials Nanoarchitectonics, National Institute for Materials Science, 1-1 Namiki, Tsukuba 305-0044, Japan

> <sup>5</sup>National Graphene Institute, University of Manchester, Booth St. E. Manchester, M13 9PL, United Kingdom

<sup>6</sup>Department of Physics and Astronomy, University of Manchester, Oxford Road, Manchester, M13 9PL, United Kingdom

(Dated: November 24, 2025)

The interaction between itinerant electrons and localized spins is key to a wide range of electronic phenomena. Of particular interest is the regime where the interacting electrons exhibit both spin and valley degeneracy, resulting in SU(4) Kondo physics. However, this regime is challenging to realize in typical mesoscopic systems because it requires a strong interaction between electrons, resulting in a Kondo temperature  $(T_{\rm K})$  significantly larger than the spin and valley splittings. Here, we present conductance measurements of a quantum point contact (QPC) in bilayer graphene (BLG). Beyond the expected quantized conductance plateaus, which reflect spin and valley degeneracy, we observe an additional subband, known as '0.7 anomaly' exhibiting signatures of Kondo physics and a  $T_{\rm K}$  ranging from approximately 0.5 up to 2.4 K at zero magnetic field, corresponding to Kondo energies between 40 and 200  $\mu$ eV. Given that the spin-orbit splitting in BLG is between 40 and 80  $\mu$ eV, we argue that these results are consistent with a transition between four-fold degenerate SU(4) and two-fold degenerate spin-valley locked SU(2) Kondo effects. Furthermore, we break the valley degeneracy of the lowest subband by an out-of-plane magnetic field and show that Kondo signatures remain present, indicating a transition from SU(4) to a valley-polarized SU(2) Kondo effect, and showing the versatility of BLG QPCs for exploring many-body effects.

Keywords: Bilayer graphene, quantum point contact, Kondo effect, 0.7 anomaly

The Kondo effect describes the interaction between moving electrons and localized spins [1], and is crucial for understanding physical phenomena as superconductivity in heavy-fermion materials [2, 3]. Its emergence in mesoscopic systems such as quantum dots [4–12] and quantum point contacts (QPCs) [13–31] has provided unprecedented control over these many-body states [32].

A QPC is a ballistic one-dimensional channel with a width comparable to the Fermi wavelength. As a result, its conductance (G) varies in steps of  $k \times \nu e^2/h$ , where  $k=1,\,2,\,\ldots$  is the subband number,  $\nu=2,\,4$  is the subband degeneracy, e is the electron charge and h is the Plank constant [33–36]. Furthermore, QPCs also show an additional subband which, in two-dimensional electron gases without valley degeneracy ( $\nu=2$ ), appears at  $G\approx 0.7\times 2e^2/h$  [37–40]. This level, which is called 0.7 anomaly, is associated with electron-electron interactions in the QPC, manifesting in Kondo- and Wigner-like physics and continues to trigger extensive theoretical and experimental work [13–31, 41].

Bilayer graphene (BLG) offers a promising platform for the exploration of Kondo physics. As a tuneable bandgap semiconductor [42–46], it has recently been introduced as a model system for the realization of electrostaticallydefined QPCs [47–54] transmitting valley-polarized electron jets [55–61] and hosting quantum dots [62, 63] showing Kondo physics [11, 12].

The small spin-orbit (SO) gap of  $40-80\,\mu\text{eV}$  [64, 65] suggests that BLG QPCs may serve as an ideal platform for exploring spin-valley degenerate SU(4) Kondo physics [10]. This regime has not yet been realized in BLG quantum dots, primarily because the Kondo temperature  $(T_{\rm K})$  at zero magnetic field is approximately 1 K and the corresponding Kondo energy  $E_{\rm K}=k_{\rm B}T_{\rm K}\approx 86\,\mu\text{eV}$ , where  $k_{\rm B}$  is the Boltzmann constant [11]; a mesoscopic system with a higher  $T_{\rm K}$  is required to explore SU(4) Kondo physics in BLG. Recent experimental work [30] has revealed a subband in BLG QPCs consistent with the 0.7 anomaly, opening new avenues for investigating Kondo physics in BLG to reach higher  $T_{\rm K}$ .

Here, we perform electronic transport experiments on a gate-defined QPC in BLG, showing spin and valley de-

<sup>\*</sup> jingla@mit.edu

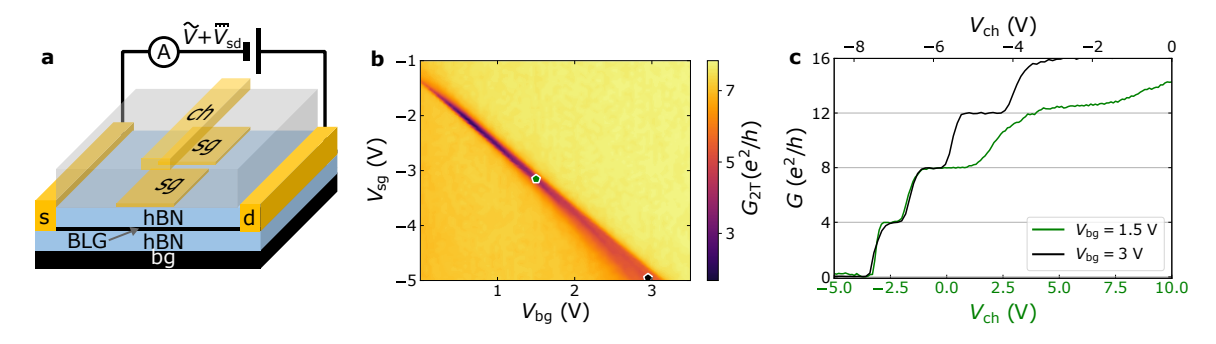


Figure 1. Gate-defined quantum point contact in BLG. (a) Device geometry: The BLG is encapsulated between atomically flat hBN insulating layers and the graphite back gate (bg) is used in combination with two Ti/Au split gates (sg) to form the QPC. The channel gate (ch) is placed on an Al<sub>2</sub>O<sub>3</sub> insulating layer to tune the QPC electrochemical potential. The contacts to the BLG are labeled as source (s) and drain (d). The circuit corresponds to the measurement geometry where  $\tilde{V}$  and  $V_{\rm sd}$  are the applied ac and dc voltages, respectively. The ammeter (A) measures the source-drain current. (b) Two-terminal conductance  $(G_{\rm 2T})$  as a function of the bg  $(V_{\rm bg})$  and sg  $(V_{\rm sg})$  voltages. The QPC conductance G is obtained from  $G_{\rm 2T}$  by subtracting the contact and ammeter resistances. (c) Channel-gate voltage  $(V_{\rm ch})$  dependence of G at  $V_{\rm bg} = 1.5$  and 3 V, corresponding to the green and black dots in panel b, respectively.

generacy ( $\nu = 4$ ). The bias dependence of G shows the activation of a level below the first subband with  $G \approx 0.7 \times 4e^2/h$  at finite bias, consistent with the 0.7 anomaly [16, 39], and a zero bias peak (ZBP) that splits under the application of an in-plane magnetic field. We show that these observations are consistent with two-fold SU(2) and four-fold degenerate SU(4) universal Kondo scaling, with activation temperatures ranging from approximately 0.5 to above 2.4 K when changing the carrier density in the QPC. As a result,  $E_{\rm K}$  becomes more than 2.5 times larger than the SO gap, indicating that the symmetry of the Kondo effect is changing from SU(2) to SU(4) [10, 66]. We further observe that a moderate outof-plane magnetic field  $(B_z)$  breaks the valley subband degeneracy. Since the temperature and bias dependence at  $B_z = 0.6$  T are consistent with Kondo physics, this result suggests that a valley-polarized Kondo regime may have been achieved.

The QPC geometry is sketched in Fig. 1a. The device is a double-gated, boron nitride (hBN)-encapsulated BLG heterostructure on a few-layer graphene back gate [49, 56] where the upper and lower hBN flakes are 28 and 23 nm thick, respectively. The split gates, with a gap of approximately 50 by 600 nm (see Supplementary Information SI note S1), were deposited on the upper hBN. The 300-nm-wide channel gate was deposited on an approximately 60-nm-thick  $\rm Al_2O_3$  layer to tune the electrochemical potential of the QPC.

Unless stated otherwise, the measurements are performed at an electron temperature of approximately 1.2 K (see SI note S2). The measurement geometry is shown in Fig. 1a, where  $\tilde{V}$  is the ac voltage bias and the ac current (I) is monitored while sweeping the back-gate  $(V_{\rm bg})$  and split-gate  $(V_{\rm sg})$  voltages. The result is shown in Fig. 1b, where the color scale represents the measured two-terminal QPC conductance,  $G_{\rm 2T} = I/\tilde{V}$ . The dark diagonal line corresponds to the charge neutrality point

of the split-gated regions and the increase in conductance with increasing  $V_{\rm bg}$  along this line is due to the formation of a QPC in between with increasing width and carrier density. We further confirm that the QPC conductance (G, obtained by subtracting the corresponding contact resistances) is quantized by fixing the  $(V_{\rm bg}, V_{\rm sg})$  voltages at (1.5, -3.35) V and (3, -5) V, corresponding to the black and green dots in Fig. 1b, and sweeping the channel gate voltage  $(V_{\rm ch})$  to deplete the QPC. As shown in Fig. 1c, as  $V_{\rm ch}$  decreases, G decreases in steps of  $4e^2/h$ , consistent with a spin and valley degenerate QPC [49].

We perform bias spectroscopy by measuring the differential conductance G as a function of  $V_{\rm ch}$  and the sourcedrain d<br/>c bias voltage  $(V_{\rm sd}).$  <br/> The result is shown in Fig. 2a for  $V_{\text{bg}}$ = 3 V, corresponding to a displacement field of approximately 0.5 V/nm [56] (see SI note S3 for  $V_{\rm bg} = 1.5$  V). For a clear subband visualization, the transconductance  $(dG/dV_{\rm ch})$  is shown in Fig. 2b, where the subbands are bright and the G plateaus appear as dark regions with corresponding subband numbers. At  $V_{\rm ch} \approx -7.58$  V, the lowest G subband, which is the 0.7 anomaly level ( $G \approx 0.7 \times 4e^2/h$  at high bias) is w-shaped near  $V_{\rm sd}=0$ . At this bias, the  $4e^2/h$  plateau extends from  $V_{\rm ch}\approx -7.45$  V to  $V_{\rm ch}\approx -6.70$  V, where an x-shaped subband structure arises due to the bias and  $V_{\rm ch}$  activation of the G = 1.5 and  $2 \times 4e^2/h$  QPC subbands [67–69]. The half-plateaus, appearing at finite bias and labeled as 0.5 and 1.5, correspond to the cases where the number of occupied QPC subbands depends on the electron propagation direction [67–69] and define a diamond-shaped structure. An additional subband appears within the lowest diamond, setting the boundary between the 0.7 anomaly level and the  $4e^2/h$  plateau. Looking back at Fig. 2a, for  $G < 4e^2/h$  one can also distinguish a conductance peak at zero  $V_{\rm sd}$  or ZBP. These observations are consistent with the 0.7 anomaly observed in GaAs-based two-dimensional electron gas systems [16, 39, 70] with G

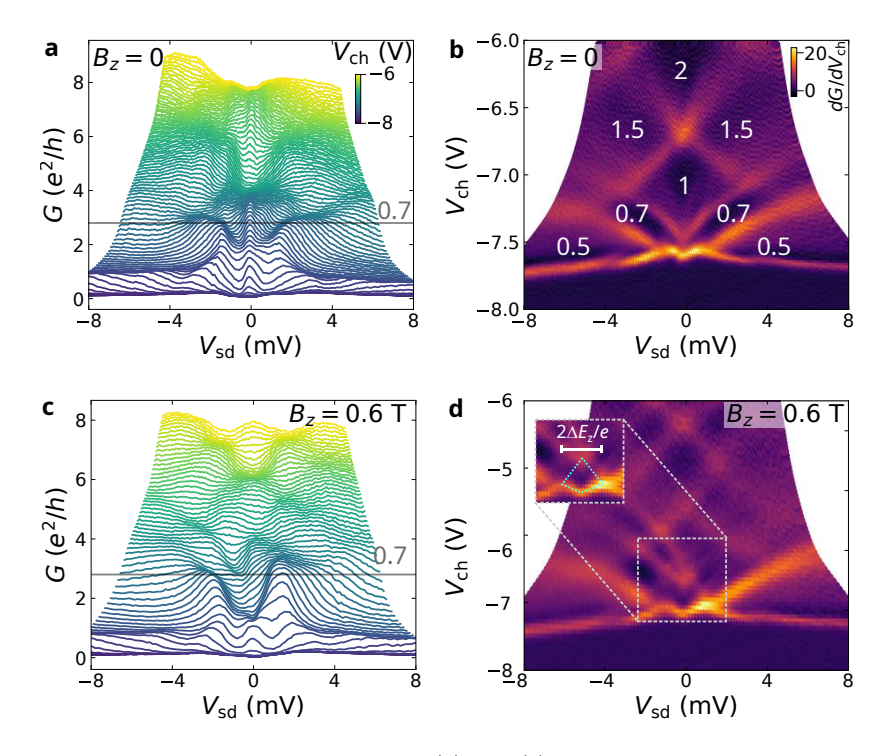


Figure 2. Bias spectroscopy of the first subband at  $V_{\rm bg} = 3$  V. (a) and (c) Bias dependence of the differential QPC conductance at  $B_{\rm z} = 0$  and 0.6 T, respectively. The line color indicates  $V_{\rm ch}$ , as shown by the color bar in a, and the horizontal line at  $G = 0.7 \times 4e^2/h$  indicates the expected position of the bias-induced plateau. (b) and (d) Transconductance  $(dG/dV_{\rm ch})$  obtained from panels a and c, respectively. The brighter regions correspond to the subbands and the darker to the plateaus, as indicated by the color bar. The white digits in b correspond to the subband numbers. The left inset in d shows the lowest subband, which is valley-split by  $\Delta E_Z \approx 1$  meV as shown by the light blue diamond.

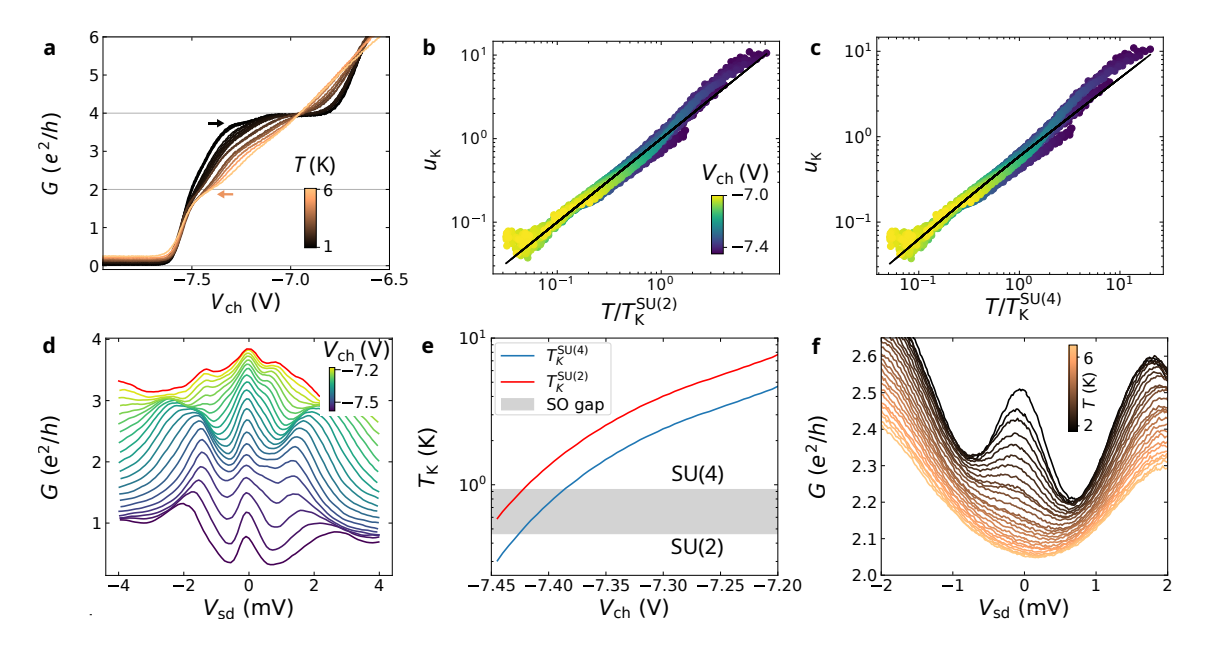


Figure 3. Temperature dependence of the QPC conductance at  $V_{\rm bg}=3$  V, zero  $V_{\rm sd}$  and zero applied magnetic field. (a)  $V_{\rm ch}$ -dependence of G at different temperatures, indicated by the line colors. (b) and (c) Universal scaling of the (b) SU(2), and (c) SU(4) Kondo function  $u_{\rm K}$  (see main text) from the fits. In panels b and c, the black line is the expected theoretical value. The dots, colored according to the color bar in b, are obtained from fits to the G vs. T data from panel a. (d) Low-bias zoom to the bias spectroscopy in Fig. 2a showing the progressive widening of the ZBP. The red trace corresponds to  $V_{\rm ch} \approx -7.18$  V, while the other traces are color-coded according to the inset colorbar. (e) SU(2) and SU(4)  $T_{\rm K}$ . At and below the gray patch, which represents the SO gap, SU(2) Kondo is expected. SU(4) is expected above the SO gap. (f) T-dependence of the ZBP. The line color indicates T, as shown by the color bar.

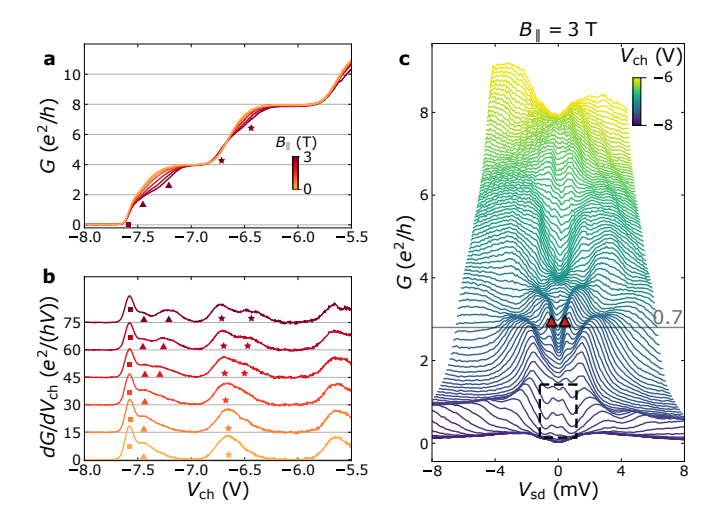


Figure 4. In-plane magnetic field effect at  $V_{\rm bg}=3$  V. (a) QPC conductance and (b) transconductance vs.  $V_{\rm ch}$  and different  $B_{\parallel}$ . The latter has been smoothed using a running average window of 15 points. The lines in both panels are color-coded according to the color bar in a. The squares indicate the 0.7 subband, the triangles and stars indicate the spin splitting of the 1 and  $2\times 4e^2/h$  subbands, respectively. (c) Bias dependence of the differential QPC conductance at  $B_{\parallel}=3$  T. The line color indicates  $V_{\rm ch}$ , as shown by the color bar, and the horizontal line at  $G=0.7\times 4e^2/h$  serves as a guide to compare with Fig. 2. The triangles indicate the accumulation of traces used to estimate the spin g-factor of the  $4e^2/h$  subband. The black rectangle highlights the splitting of the zero-bias peak.

now being two times larger due to the spin and valley degeneracy.

Due to the large valley g factor of BLG QPCs [71], a small out-of-plane magnetic field  $(B_z)$  suffices to break the valley degeneracy in the QPC. This result is shown in Figs. 2c and 2d. As shown by the light blue diamond in panel d, the first subband is valley-split by  $\Delta E_Z \approx 1$  meV, which is larger than  $E_K$  for  $T_K < 10$  K. In Fig. 2c, near  $4e^2/h$ , the ZBP acquires a strong antisymmetric component. We attribute such a shape to a Fano effect which is compatible with Kondo physics [72]. We thus conclude that Figs. 2c and 2d are consistent with valley-polarized SU(2) Kondo (see SI Section S5 for the detailed analysis of the  $B_z = 0.6$  T data in terms of Kondo and Fano physics).

An important feature of the Kondo effect in QPCs is that G decreases with increasing temperature (T) [16, 38, 39]. Figure 3a shows that, at  $V_{\rm sd}=0$ , G decreases with increasing T and a short plateau appears slightly below  $G=2e^2/h$  (copper arrow), similar to a result in Si/SiGe [41]. We have fit the G vs. T data to a rescaled Kondo model [16]:  $G_{\rm K}=G_{\rm min}+(G_{\rm max}-G_{\rm min})f_{\rm K}(T/T_{\rm K})$ , where  $G_{\rm max}=4e^2/h$ ,  $G_{\rm min}=1.4e^2/h$  (see SI note S4) is the minimal QPC conductance at high temperature and  $f_{\rm K}=[1+(2^{1/s}-1)^{2/n}(T/T_{\rm K})^2]^{-s}$  is the Kondo activation function, where s=0.22 and n=2 for SU(2) [7] and s=0.2 and n=3 for SU(4) Kondo physics

[10]. Following Ref. [22], we have plotted the universal Kondo  $u_{\rm K}=\sqrt{\frac{G_{\rm r}^{-1/s}-1}{2^{1/s}-1}}$  scaling function, where  $G_{\rm r}=\frac{G-G_{\rm min}}{G_{\rm max}-G_{\rm min}}$ . The results are displayed in Figs. 3b and 3c and show that both SU(2) and SU(4) Kondo scalings are compatible with our data (see SI Note S4 for the universal scaling of G vs.  $T/T_{\rm K}$ ). For clarity, the SU(2) and SU(4)  $T_{\rm K}$  are labeled as  $T_{\rm K}^{\rm SU(2)}$  and  $T_{\rm K}^{\rm SU(4)}$ , respectively.

The additional plateau observed in Fig. 3a when G is slightly below  $4e^2/h$  and at the lowest T (black arrow) resembles the effect of bound states introduced in Ref. [22] in a similar one-dimensional geometry. There, two small protrusions were introduced in different spots on the split gate structure and, in addition to a plateau, a decrease in G below the first subband was observed for T > 0.2 K, an indication of the formation of a bound state. In our case,  $dG/dV_{\rm ch}$  does not change sign at higher T. Owning to the large aspect ratio of our QPC, this may originate from irregularities at the split-gate edges, consistent with different observations in SI Notes S1, S3, and S5.

The application of a  $V_{\rm sd}$  breaks the Kondo state at a characteristic bias, which is determined by  $E_{\rm K}$  [6, 7, 16]. Figure 3d is a low  $V_{\rm sd}$  zoom to Fig. 2a that shows the ZBPs, and their apparent broadening with increasing  $V_{\rm ch}$ . At high  $V_{\rm ch}$  values (see red trace), an oscillation emerges within the ZBP, indicating interference effects may influence the low  $V_{\rm sd}$  G in these conditions. Figure 3e shows that  $T_{\rm K}$  increases with  $V_{\rm ch}$ , consistent with the ZBP width. In addition, both  $T_{\rm K}^{\rm SU(2)}$  and  $T_{\rm K}^{\rm SU(4)}$  range from values comparable to the SO gap at low  $V_{\rm ch}$  to significantly greater magnitudes (Fig. 3e), suggesting a transition from SU(2) to SU(4) physics. Independent evidence for the relatively high  $T_{\rm K}$  is obtained from the T-dependent ZBP obtained in a different cooldown and shown in Fig. 3f. Its persistence beyond 2.8 K and the absence of a clear broadening indicate that the Kondo temperature lies well above 1 K [4, 8].

We now explore the effect of an in-plane magnetic field  $(B_{\parallel})$  on the subband structure. Figure 4a shows the  $V_{\text{ch}}$ -dependence of the QPC conductance at different  $B_{\parallel}$ (indicated by the line color). As expected, new kinks appear at the subband locations when increasing  $B_{\parallel}$ , indicating additional spin splittings. To visualize them, Fig. 4b shows  $dG/dV_{\rm ch}$  at different  $B_{\parallel},$  which is colorcoded according to Fig. 4a. One observes that, while the  $G = 2 \times 4e^2/h$  subband at  $B_{\parallel} = 3$  T is split into two (stars), the 0.7 anomaly (squares) and  $1 \times 4e^2/h$ (right triangles) subbands remain separated, and an additional subband appears between them (left triangles), resulting in three transconductance peaks, in agreement with Ref. [30]. We attribute the latter to the spin splitting of the  $4e^2/h$  subband. In Fig. 4c, we characterize the QPCs bias dependence at  $B_{\parallel} = 3$  T and confirm the presence of the new conductance level, visible as a dense accumulation of traces with finite bias that saturates approximately at  $4e^2/h$ . The wing shape of this subband,

which ranges from  $0.3 < |V_{\rm sd}| < 0.6$  mV (Fig. 4c, red triangles), is caused by the spin splitting of the  $4e^2/h$  level. Following Ref. [16], we use this range to estimate the spin g-factor, which is  $g = 2.6 \pm 0.9$ , in agreement with the g = 2 obtained in graphene [64, 73]. In addition, the high  $V_{\rm sd}$  tails saturating slightly above  $G = 0.7 \times 4e^2/h$  remain unchanged by  $B_{\parallel}$  up to 8 T (see SI note S6), an indication of the robustness of the 0.7 anomaly state at finite bias.

Finally, we analyze the ZBPs highlighted by the dashed rectangle in Fig. 4c. Their splitting is a signature of the Kondo effect [7, 16]. Assuming that the peak separation is proportional to  $2g^*\mu_{\rm B}B$ , we obtain  $g^*=2\pm0.5$ , consistent with the splitting of a spin 1/2 electronic state responsible for the Kondo effect [5]. However, for G higher than  $2e^2/h$  and temperatures above 1.7 K, we find that the ZBP disappears with  $B_{\parallel}$  (see SI note S8). Such a ZBP behavior is consistent with previous reports on GaAs/AlGaAs QPCs [16, 26].

To conclude, we have performed transport experiments on a BLG-based QPC, showing several features consistent with the Kondo effect. These include universal scaling of G vs. T, a subband below  $4e^2/h$  evolving towards  $G \approx 0.7 \times 4e^2/h$  at finite bias, and a ZBP that splits under  $B_{\parallel}$  and has a width that scales like  $T_{\rm K}$ . Since  $E_{\rm K}$  spans values comparable to the spin-orbit gap and extends to more than 2.5 times its magnitude, we conclude that the Kondo degeneracy evolves from SU(2) to SU(4). In addition, we break the valley degeneracy by applying an out-of-plane magnetic field and show signatures of Kondo effects in this regime. Our results show the relevance of Kondo physics in BLG QPCs and allow us to study the effects of valley degeneracy on the Kondo physics in the small SO coupling range [11, 12], enabling

different transitions from SU(2) to SU(4) Kondo physics.

Note added: We just became aware of a related work where the 0.7 anomaly in BLG QPCs is investigated when breaking the four-fold degeneracy by proximity-induced spin-valley coupling [74].

#### ACKNOWLEDGEMENTS

We thank Prof. K. Ensslin, H. Duprez, A.R.L. Manesco, and P. Stevic for insightful discussions. This project received funding from the European Union Horizon 2020 research and innovation program under grant agreement no. 863098 (SPRING). J.I-A acknowledges support from the European Commission for a Marie Sklodowska–Curie individual fellowship No. 101027187-PCSV, T.S.G. acknowledges support from the Dutch Research Council (NWO) for a Rubicon grant (Project No. 019.222EN.013), K.W. and T.T. acknowledge support from JSPS KAKENHI (Grant Numbers 19H05790, 20H00354 and 21H05233). A.K. acknowledges support from the Deutsche Forschungsgemeinschaft (DFG, German Research Foundation) within DFG Individual Grants KN 1383/4 (Project-ID 529637137), KN 1383/7 (Project-ID 555830897), and SFB 1277 Project A07 (Project-ID 314695032). Collaboration aspect of this project was supported by the International Science Partnerships Fund (UK).

### DATA AVAILABILITY

All the data and code associated with the analysis are available at [75].

- [1] J. Kondo, Resistance minimum in dilute magnetic alloys, Progress of theoretical physics **32**, 37 (1964).
- [2] S. G. Stewart, Heavy-fermion systems, Reviews of Modern Physics 56, 755 (1984).
- [3] W. Zhao, B. Shen, Z. Tao, Z. Han, K. Kang, K. Watanabe, T. Taniguchi, K. F. Mak, and J. Shan, Gate-tunable heavy fermions in a moiré kondo lattice, Nature 616, 61 (2023).
- [4] L. I. Glazman and M. E. Raikh, Resonant kondo transparency of a barrier with quasilocal impurity states, JETP Letters 47, 452 (1988).
- [5] D. Goldhaber-Gordon, H. Shtrikman, D. Mahalu, D. Abusch-Magder, U. Meirav, and M. Kastner, Kondo effect in a single-electron transistor, Nature 391, 156 (1998).
- [6] S. M. Cronenwett, T. H. Oosterkamp, and L. P. Kouwenhoven, A tunable kondo effect in quantum dots, Science 281, 540 (1998).
- [7] D. Goldhaber-Gordon, J. Göres, M. Kastner, H. Shtrikman, D. Mahalu, and U. Meirav, From the kondo regime to the mixed-valence regime in a single-electron transis-

- tor, Physical Review Letters 81, 5225 (1998).
- [8] W. Van der Wiel, S. D. Franceschi, T. Fujisawa, J. Elzerman, S. Tarucha, and L. Kouwenhoven, The kondo effect in the unitary limit, Science 289, 2105 (2000).
- [9] P. Jarillo-Herrero, J. Kong, H. S. Van Der Zant, C. Dekker, L. P. Kouwenhoven, and S. De Franceschi, Orbital kondo effect in carbon nanotubes, Nature 434, 484 (2005).
- [10] A. Keller, S. Amasha, I. Weymann, C. Moca, I. Rau, J. Katine, H. Shtrikman, G. Zaránd, and D. Goldhaber-Gordon, Emergent su (4) kondo physics in a spin-chargeentangled double quantum dot, Nature Physics 10, 145 (2014).
- [11] A. Kurzmann, Y. Kleeorin, C. Tong, R. Garreis, A. Knothe, M. Eich, C. Mittag, C. Gold, F. K. de Vries, K. Watanabe, et al., Kondo effect and spin-orbit coupling in graphene quantum dots, Nature Communications 12, 6004 (2021).
- [12] C. Tong, A. Kurzmann, R. Garreis, K. Watanabe, T. Taniguchi, T. Ihn, and K. Ensslin, Pauli blockade catalogue and three-and four-particle kondo effect in bi-

- layer graphene quantum dots, Physical Review Research 6, L012006 (2024).
- [13] C. Kane and M. P. Fisher, Transmission through barriers and resonant tunneling in an interacting one-dimensional electron gas, Physical Review B 46, 15233 (1992).
- [14] Y. Oreg and A. M. Finkel'stein, dc transport in quantum wires, Physical Review B 54, R14265 (1996).
- [15] O. Sushkov, Conductance anomalies in a one-dimensional quantum contact, Physical Review B 64, 155319 (2001).
- [16] S. Cronenwett, H. Lynch, D. Goldhaber-Gordon, L. Kouwenhoven, C. Marcus, K. Hirose, N. Wingreen, and V. Umansky, Low-temperature fate of the 0.7 structure in a point contact: A kondo-like correlated state in an open system, Physical Review Letters 88, 226805 (2002).
- [17] Y. Meir, K. Hirose, and N. S. Wingreen, Kondo model for the "0.7 anomaly" in transport through a quantum point contact, Physical Review Letters 89, 196802 (2002).
- [18] P. Roche, J. Ségala, D. Glattli, J. Nicholls, M. Pepper, A. Graham, K. Thomas, M. Simmons, and D. Ritchie, Fano factor reduction on the 0.7 conductance structure of a ballistic one-dimensional wire, Physical Review Letters 93, 116602 (2004).
- [19] L. DiCarlo, Y. Zhang, D. McClure, D. Reilly, C. Marcus, L. Pfeiffer, and K. West, Shot-noise signatures of 0.7 structure and spin in a quantum point contact, Physical Review Letters 97, 036810 (2006).
- [20] T. Rejec and Y. Meir, Magnetic impurity formation in quantum point contacts, Nature 442, 900 (2006).
- [21] E. Koop, A. Lerescu, J. Liu, B. Van Wees, D. Reuter, A. Wieck, and C. Van Der Wal, The influence of device geometry on many-body effects in quantum point contacts: signatures of the 0.7 anomaly, exchange and kondo, Journal of superconductivity and novel magnetism 20, 433 (2007).
- [22] F. Sfigakis, C. Ford, M. Pepper, M. Kataoka, D. Ritchie, and M. Simmons, Kondo effect from a tunable bound state within a quantum wire, Physical Review Letters 100, 026807 (2008).
- [23] S. Sarkozy, F. Sfigakis, K. Das Gupta, I. Farrer, D. Ritchie, G. Jones, and M. Pepper, Zero-bias anomaly in quantum wires, Physical Review B—Condensed Matter and Materials Physics 79, 161307 (2009).
- [24] Y. Ren, W. Yu, S. Frolov, J. Folk, and W. Wegscheider, Zero-bias anomaly of quantum point contacts in the low-conductance limit, Physical Review B—Condensed Matter and Materials Physics 82, 045313 (2010).
- [25] N. Tombros, A. Veligura, J. Junesch, M. H. Guimarães, I. J. Vera-Marun, H. T. Jonkman, and B. J. Van Wees, Quantized conductance of a suspended graphene nanoconstriction, Nature Physics 7, 697 (2011).
- [26] M. Iqbal, R. Levy, E. Koop, J. Dekker, J. De Jong, J. Van Der Velde, D. Reuter, A. Wieck, R. Aguado, Y. Meir, et al., Odd and even kondo effects from emergent localization in quantum point contacts, Nature 501, 79 (2013).
- [27] F. Bauer, J. Heyder, E. Schubert, D. Borowsky, D. Taubert, B. Bruognolo, D. Schuh, W. Wegscheider, J. von Delft, and S. Ludwig, Microscopic origin of the '0.7-anomaly' in quantum point contacts, Nature 501, 73 (2013).
- [28] B. Brun, F. Martins, S. Faniel, B. Hackens, G. Bachelier, A. Cavanna, C. Ulysse, A. Ouerghi, U. Gennser, D. Mailly, et al., Wigner and kondo physics in quantum point contacts revealed by scanning gate microscopy, Na-

- ture communications 5, 4290 (2014).
- [29] J. Heyder, F. Bauer, E. Schubert, D. Borowsky, D. Schuh, W. Wegscheider, J. Von Delft, and S. Ludwig, Relation between the 0.7 anomaly and the kondo effect: Geometric crossover between a quantum point contact and a kondo quantum dot, Physical Review B 92, 195401 (2015).
- [30] V. Gall, R. Kraft, I. V. Gornyi, and R. Danneau, Spin and valley degrees of freedom in a bilayer graphene quantum point contact: Zeeman splitting and interaction effects, Physical Review Research 4, 023142 (2022).
- [31] J. Hong, Gate-voltage-driven quantum phase transition at  $0.7(2e^2/h)$  in quantum point contacts, arXiv preprint arXiv:2502.18850 (2025).
- [32] L. Kouwenhoven and L. Glazman, Revival of the kondo effect, Physics World 14, 33 (2001).
- [33] B. Van Wees, H. Van Houten, C. Beenakker, J. G. Williamson, L. Kouwenhoven, D. Van der Marel, and C. Foxon, Quantized conductance of point contacts in a two-dimensional electron gas, Physical Review Letters 60, 848 (1988).
- [34] D. Wharam, T. J. Thornton, R. Newbury, M. Pepper, H. Ahmed, J. Frost, D. Hasko, D. Peacock, D. Ritchie, and G. Jones, One-dimensional transport and the quantisation of the ballistic resistance, Journal of Physics C: solid state physics 21, L209 (1988).
- [35] L. I. Glazman, G. B. Lesovik, D. Khmel'nitskii, and R. I. Shekhter, Reflectionless quantum transport and fundamental ballistic-resistance steps in microscopic constrictions, Pis'ma Zh. Eksp. Teor. Fiz. 48, 218 (1988).
- [36] C. Beenakker and H. van Houten, Quantum transport in semiconductor nanostructures, in *Solid State Physics*, Vol. 44 (Elsevier, 1991) pp. 1–228.
- [37] K. Thomas, J. Nicholls, M. Simmons, M. Pepper, D. Mace, and D. Ritchie, Possible spin polarization in a one-dimensional electron gas, Physical Review Letters 77, 135 (1996).
- [38] A. Kristensen, P. Lindelof, J. B. Jensen, M. Zaffalon, J. Hollingbery, S. Pedersen, J. Nygård, H. Bruus, S. Reimann, C. Sørensen, et al., Temperature dependence of the "0.7" 2e2/h quasi-plateau in strongly confined quantum point contacts, Physica B: Condensed Matter 249, 180 (1998).
- [39] A. Kristensen, H. Bruus, A. Hansen, J. Jensen, P. Lindelof, C. Marckmann, J. Nygård, C. Sørensen, F. Beuscher, A. Forchel, et al., Bias and temperature dependence of the 0.7 conductance anomaly in quantum point contacts, Physical Review B 62, 10950 (2000).
- [40] L. Rokhinson, L. Pfeiffer, and K. West, Spontaneous spin polarization in quantum point contacts, Physical Review Letters **96**, 156602 (2006).
- [41] J. Von Pock, D. Salloch, G. Qiao, U. Wieser, T. Hackbarth, and U. Kunze, Quantization and anomalous structures in the conductance of si/sige quantum point contacts, Journal of Applied Physics 119 (2016).
- [42] E. V. Castro, K. Novoselov, S. Morozov, N. Peres, J. L. Dos Santos, J. Nilsson, F. Guinea, A. Geim, and A. C. Neto, Biased bilayer graphene: semiconductor with a gap tunable by the electric field effect, Physical Review Letters 99, 216802 (2007).
- [43] J. B. Oostinga, H. B. Heersche, X. Liu, A. F. Morpurgo, and L. M. Vandersypen, Gate-induced insulating state in bilayer graphene devices, Nature Materials 7, 151 (2008).
- [44] Y. Zhang, T.-T. Tang, C. Girit, Z. Hao, M. C. Martin, A. Zettl, M. F. Crommie, Y. R. Shen, and F. Wang,

- Direct observation of a widely tunable bandgap in bilayer graphene, Nature **459**, 820 (2009).
- [45] E. Icking, L. Banszerus, F. Wörtche, F. Volmer, P. Schmidt, C. Steiner, S. Engels, J. Hesselmann, M. Goldsche, K. Watanabe, et al., Transport spectroscopy of ultraclean tunable band gaps in bilayer graphene, Advanced Electronic Materials , 2200510 (2022).
- [46] L. Seemann, A. Knothe, and M. Hentschel, Gate-tunable regular and chaotic electron dynamics in ballistic bilayer graphene cavities, Physical Review B 107, 205404 (2023).
- [47] M. T. Allen, J. Martin, and A. Yacoby, Gate-defined quantum confinement in suspended bilayer graphene, Nature Communications 3, 1 (2012).
- [48] A. S. M. Goossens, S. C. Driessen, T. A. Baart, K. Watanabe, T. Taniguchi, and L. M. Vandersypen, Gate-defined confinement in bilayer graphene-hexagonal boron nitride hybrid devices, Nano Letters 12, 4656 (2012).
- [49] H. Overweg, H. Eggimann, X. Chen, S. Slizovskiy, M. Eich, R. Pisoni, Y. Lee, P. Rickhaus, K. Watanabe, T. Taniguchi, et al., Electrostatically induced quantum point contacts in bilayer graphene, Nano Letters 18, 553 (2018).
- [50] R. Kraft, J. Mohrmann, R. Du, P. B. Selvasundaram, M. Irfan, U. N. Kanilmaz, F. Wu, D. Beckmann, H. Von Löhneysen, R. Krupke, et al., Tailoring supercurrent confinement in graphene bilayer weak links, Nature Communications 9, 1722 (2018).
- [51] A. Knothe and V. Fal'ko, Influence of minivalleys and berry curvature on electrostatically induced quantum wires in gapped bilayer graphene, Physical Review B 98, 155435 (2018).
- [52] H. Overweg, A. Knothe, T. Fabian, L. Linhart, P. Rickhaus, L. Wernli, K. Watanabe, T. Taniguchi, D. Sánchez, J. Burgdörfer, et al., Topologically nontrivial valley states in bilayer graphene quantum point contacts, Physical Review Letters 121, 257702 (2018).
- [53] R. Kraft, I. Krainov, V. Gall, A. Dmitriev, R. Krupke, I. Gornyi, and R. Danneau, Valley subband splitting in bilayer graphene quantum point contacts, Physical Review Letters 121, 257703 (2018).
- [54] T. L. Lane, A. Knothe, and V. I. Fal'ko, Semimetallic features in quantum transport through a gate-defined point contact in bilayer graphene, Physical Review B 100, 115427 (2019).
- [55] C. Gold, A. Knothe, A. Kurzmann, A. Garcia-Ruiz, K. Watanabe, T. Taniguchi, V. Fal'ko, K. Ensslin, and T. Ihn, Coherent jetting from a gate-defined channel in bilayer graphene, Physical Review Letters 127, 046801 (2021).
- [56] J. Ingla-Aynés, A. L. Manesco, T. S. Ghiasi, S. Volosheniuk, K. Watanabe, T. Taniguchi, and H. S. van der Zant, Specular electron focusing between gate-defined quantum point contacts in bilayer graphene, Nano Letters 23, 5453 (2023).
- [57] J. Ingla-Aynés, A. L. Manesco, T. S. Ghiasi, K. Watanabe, T. Taniguchi, and H. S. Van Der Zant, Ballistic electron source with magnetically controlled valley polarization in bilayer graphene, Physical Review Letters 133, 156301 (2024).
- [58] K. Huang, H. Fu, K. Watanabe, T. Taniguchi, and J. Zhu, High-temperature quantum valley hall effect with quantized resistance and a topological switch, Science 385,

- 657 (2024).
- [59] K. Davydov, X. Zhang, W. Ren, M. Coles, L. Kline, B. Zucker, K. Watanabe, T. Taniguchi, and K. Wang, Easy-to-configure zero-dimensional valley-chiral modes in a graphene point junction, Science Advances 10, eadp6296 (2024).
- [60] J. D. Torres Luna, K. Vilkelis, and A. L. Manesco, Probing valley phenomena with gate-defined valley splitters, SciPost Physics 18, 062 (2025).
- [61] A. L. Manesco and A. Pulkin, Spatial separation of spin currents in transition metal dichalcogenides, SciPost Physics Core 6, 036 (2023).
- [62] M. Eich, F. Herman, R. Pisoni, H. Overweg, A. Kurzmann, Y. Lee, P. Rickhaus, K. Watanabe, T. Taniguchi, M. Sigrist, et al., Spin and valley states in gate-defined bilayer graphene quantum dots, Physical Review X 8, 031023 (2018).
- [63] L. Banszerus, B. Frohn, A. Epping, D. Neumaier, K. Watanabe, T. Taniguchi, and C. Stampfer, Gatedefined electron-hole double dots in bilayer graphene, Nano Letters 18, 4785 (2018).
- [64] L. Banszerus, B. Frohn, T. Fabian, S. Somanchi, A. Epping, M. Müller, D. Neumaier, K. Watanabe, T. Taniguchi, F. Libisch, et al., Observation of the spinorbit gap in bilayer graphene by one-dimensional ballistic transport, Physical Review Letters 124, 177701 (2020).
- [65] H. Duprez, S. Cances, A. Omahen, M. Masseroni, M. J. Ruckriegel, C. Adam, C. Tong, R. Garreis, J. D. Gerber, W. Huang, et al., Spin-valley locked excited states spectroscopy in a one-particle bilayer graphene quantum dot, Nature Communications 15, 9717 (2024).
- [66] A. Kurzmann, H. Overweg, M. Eich, A. Pally, P. Rickhaus, R. Pisoni, Y. Lee, K. Watanabe, T. Taniguchi, T. Ihn, et al., Charge detection in gate-defined bilayer graphene quantum dots, Nano Letters 19, 5216 (2019).
- [67] L. I. Glazman and A. V. Khaetskii, Nonlinear quantum conductance of a point contact, Pis'ma Zh. Eksp. Teor. Fiz. 48, 546 (1988).
- [68] L. Kouwenhoven, B. Van Wees, C. Harmans, J. Williamson, H. Van Houten, C. Beenakker, C. Foxon, and J. Harris, Nonlinear conductance of quantum point contacts, Physical Review B 39, 8040 (1989).
- [69] N. Patel, J. Nicholls, L. Martín-Moreno, M. Pepper, J. Frost, D. Ritchie, and G. Jones, Evolution of half plateaus as a function of electric field in a ballistic quasi-one-dimensional constriction, Physical Review B 44, 13549 (1991).
- [70] K. Thomas, J. Nicholls, N. Appleyard, M. Simmons, M. Pepper, D. Mace, W. Tribe, and D. Ritchie, Interaction effects in a one-dimensional constriction, Physical Review B 58, 4846 (1998).
- [71] Y. Lee, A. Knothe, H. Overweg, M. Eich, C. Gold, A. Kurzmann, V. Klasovika, T. Taniguchi, K. Wantanabe, V. Fal'ko, et al., Tunable valley splitting due to topological orbital magnetic moment in bilayer graphene quantum point contacts, Physical Review Letters 124, 126802 (2020).
- [72] B. R. Bułka and P. Stefański, Fano and kondo resonance in electronic current through nanodevices, Physical Review Letters 86, 5128 (2001).
- [73] T. J. Lyon, J. Sichau, A. Dorn, A. Centeno, A. Pesquera, A. Zurutuza, and R. H. Blick, Probing electron spin resonance in monolayer graphene, Physical Review Letters 119, 066802 (2017).

- [74] J. D. Gerber, E. Ersoy, M. Masseroni, M. Niese, A. O. Denisov, C. Adam, L. Ostertag, J. Richter, T. Taniguchi, K. Watanabe, Y. Meir, T. Ihn, and K. Ensslin, Gate-tunable regular and chaotic electron dynamics in ballistic bilayer graphene cavities, arXiv preprint arXiv:2511.06384 (2025).
- [75] J. Ingla-Aynés, S. Volosheniuk, T. S. Ghiasi, A. Knothe, K. Watanabe, T. Taniguchi, V. I. Fal'ko, and H. S. J. van der Zant, Data underlying the publication: Tuneable kondo effect in a bilayer graphene quantum channel, https://doi.org/10.4121/3a635068-b309-4b71-b2c8-587bb01752c3 (2025).
- [76] M. Gruber, A. Weismann, and R. Berndt, The kondo resonance line shape in scanning tunnelling spectroscopy: instrumental aspects, Journal of Physics: Condensed Matter 30, 424001 (2018).
- [77] B. J. van Wees, L. Kouwenhoven, E. Willems, C. Harmans, J. Mooij, H. Van Houten, C. Beenakker, J. Williamson, and C. Foxon, Quantum ballistic and adiabatic electron transport studied with quantum point contacts, Physical Review B 43, 12431 (1991).
- [78] J. Göres, D. Goldhaber-Gordon, S. Heemeyer, M. Kastner, H. Shtrikman, D. Mahalu, and U. Meirav, Fano resonances in electronic transport through a single-electron transistor, Physical Review B 62, 2188 (2000).

# **Supplementary Information**

### CONTENTS

	Acknowledgements	5
	Data availability	5
	References	5
S1.	Device geometry	1
S2.	Electronic measurements	2
S3.	QPC formation at different electric fields	2
S4.	$G_{\min}$ dependence of the Kondo analysis	3
S5.	Temperature dependent transport with $B_z=0.6~\mathrm{T}$ and Fano physics	4
S6.	In-plane magnetic field dependence in a different cooldown	5
S7.	Temperature dependence of zero-bias peak	6
S8.	Magnetic field dependence of zero-bias peak	6
S9.	Determination of the valley $q$ factor	7

### S1. DEVICE GEOMETRY

Figure S1a is a sketch of the measured device, and Fig. S1b shows an atomic force microscopy image taken before depositing the  $Al_2O_3$ . The image shows imperfections at the split gate edges, which are consistent with our observations in the main manuscript and Sections S3 and S5.

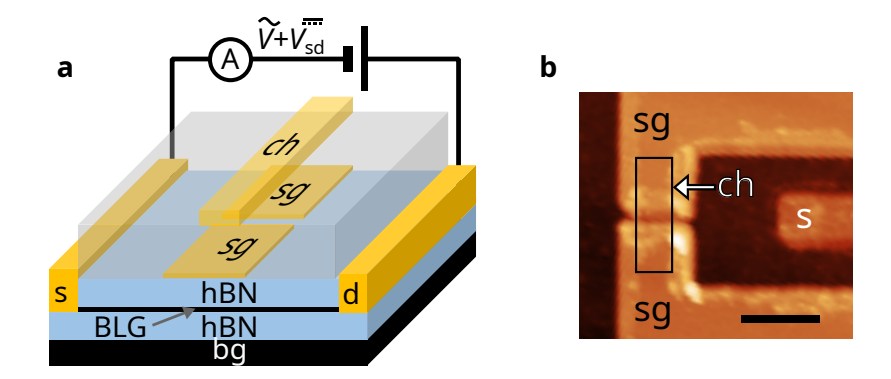


Figure S1. (a) Schematic of the measured device where the graphite back gate (bg) and bilayer graphene (BLG) are black, the hexagonal boron nitride (hBN) flakes are light blue, the Ti/Au split gates (sg), the channel gate (ch), and the source (s) and drain (d) contacts are golden, and the  $Al_2O_3$  layer under ch is semi-transparent. (b) Atomic force microscopy of the device before channel gate preparation. Its approximate position is indicated by the rectangle. The scale bar is  $0.6 \mu m$ .

### S2. ELECTRONIC MEASUREMENTS

To obtain clean data, we applied an ac voltage  $\tilde{V}=100~\mu\mathrm{V}$  to our sample. To estimate the electron temperature (T), we have used  $T=\sqrt{T_l^2+(e\tilde{V}/k_\mathrm{B})^2}$ , where  $T_l$  is the lattice temperature, e is the electron charge,  $k_\mathrm{B}$  is the Boltzmann constant, and  $e\tilde{V}/k_\mathrm{B}\approx 0.96~\mathrm{K}$ . The validity of this approximation is confirmed by the fact that the temperature-dependent analysis yields very similar results when the data obtained at the lowest temperatures are not used.

In the measurement circuit, which is shown in Fig. S1a, one can see that the resistances of the electrodes and the ammeter are also measured and need to be subtracted to obtain the conductance (G) of the quantum point contact (QPC). The ammeter resistance, which was measured separately, is 3 k $\Omega$ . The contact resistances depend on the backgate voltage  $(V_{bg})$ , and are 377  $\Omega$  and 570  $\Omega$  at  $V_{bg}=3$  and 1.5 V, respectively. These values are, respectively, 100  $\Omega$  and 250  $\Omega$  larger than the values obtained by setting the split gate voltage to zero and were extracted by setting the lowest QPC subband to  $G=4e^2/h$ , where e is the electron charge and h the Plank constant. We attribute these small differences to the effect of QPC areas not covered by the channel gate. Note that the contact resistances are significantly smaller than typical QPC resistances  $(h/4e^2 \approx 6.4 \,\mathrm{k}\Omega)$  in our experiment.

### S3. QPC FORMATION AT DIFFERENT ELECTRIC FIELDS

Figure S2 shows the dc bias  $(V_{\rm sd})$  and channel gate voltage  $(V_{\rm ch})$  dependence of G at a back gate voltage  $V_{\rm bg}=3$  and 1.5 V. The zero-bias peak (ZBP) height at low G is less pronounced at  $V_{\rm bg}=1.5$  V than at 3 V. Looking at Fig. S2d, one can also observe that, at zero  $V_{\rm sd}$ , the separation between the 0.7 and  $1\times 4e^2/h$  subbands is more pronounced than in Fig. S2b. Finally, a zigzag pattern is observed in the transconductance plot at  $V_{\rm bg}=1.5$  V for low  $V_{\rm sd}$  and below the  $4e^2/h$  subband. We attribute this structure to faint Coulomb diamonds. They indicate that weakly confined quantum dots may form within the QPC. Since the potential inside BLG QPCs is not flat [49], its depth at the center depends on the width. This implies that having a varying QPC width due to rough split gate edges may result in weakly confined areas in the QPC under certain conditions.

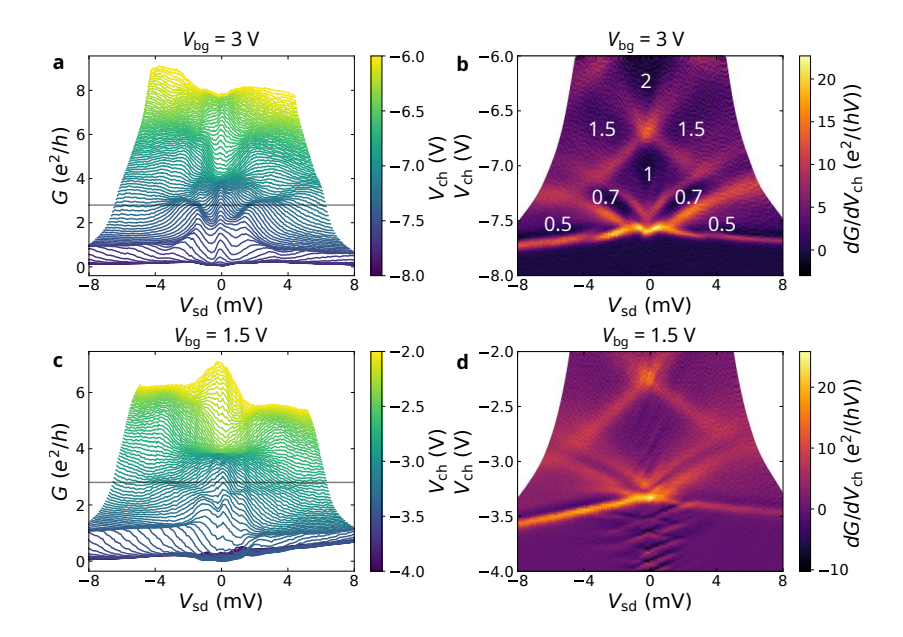


Figure S2. (a) and (c) Bias  $(V_{\rm sd})$ -dependence of the QPC conductance (G) at different channel gate voltages  $(V_{\rm ch})$ , indicated by the line colors. The gray lines show  $G = 0.7 \times 4e^2/h$ , where the 0.7 anomaly is expected. (b) and (d) Transconductance  $dG/dV_{\rm ch}$  vs.  $V_{\rm sd}$  and  $V_{\rm ch}$  obtained from panels a and c, respectively.

### S4. $G_{\min}$ DEPENDENCE OF THE KONDO ANALYSIS

According to the Kondo model used here [16], the QPC conductance follows

$$G_{K} = G_{\min} + (G_{\max} - G_{\min}) f_{K}(T/T_{K}), \tag{S1}$$

where  $G_{\text{max}} = 4e^2/h$ ,  $G_{\text{min}}$  is the minimal QPC conductance at high temperature,  $f_{\text{K}} = [1 + (2^{1/s} - 1)(T/T_{\text{K}})^2]^{-s}$  is the Kondo activation function,  $T_{\text{K}}$  the Kondo temperature and s = 0.22, corresponding to SU(2) Kondo [7, 16].

Given that  $G_{\min}$  is the only free parameter besides  $T_{\rm K}$ , one might question the robustness of the observed universal scaling and the correlation between  $T_{\rm K}$  and the bias activation of the 0.7 anomaly band to variations in  $G_{\min}$ . For this reason, in Fig. S3 we show the  $G_{\min}$  dependence of the universal Kondo scaling function

$$u_{\rm K} = \sqrt{\frac{G_{\rm r}^{-1/s} - 1}{2^{1/s} - 1}},$$
 (S2)

where  $G_{\rm r}=\frac{G-G_{\rm min}}{G_{\rm max}-G_{\rm min}}$ . Note that, in the ideal case  $G_{\rm r}=f_{\rm K}$  and  $u_{\rm K}=T/T_{\rm K}$ .

To illustrate the effect of  $G_{\min}$ , Figs. S3a-S3e show the SU(2) Kondo universal scaling for  $0.5e^2/h < G_{\min} < 2e^2/h$ , where one can see that the best agreement between the universal scaling curves (black lines) and the values extracted from the experiment (dots colored according to the color bar in Fig. S3a) occur in the range  $e^2/h < G_{\min} < 1.5e^2/h$ . Figure S3f shows the bias dependence of the lowest QPC subband transconductance at  $V_{\rm bg} = 3$  V. The white and yellow curves show  $2k_{\rm B}T_{\rm K}/e$  vs.  $V_{\rm ch}$  for  $G_{\min} = 0$  and  $2e^2/h$ , respectively, and show that  $T_{\rm K}$  is only weakly sensitive to changes in  $G_{\min}$ . As a consequence, the agreement between both measurements is not affected by the choice of  $G_{\min}$ . For completeness, the inset of Fig. S3d shows the universal scaling of G vs.  $T/T_{\rm K}$ , as reported in Ref. [16] for  $G_{\min} = 1.4e^2/h$ , the value used in the main manuscript.

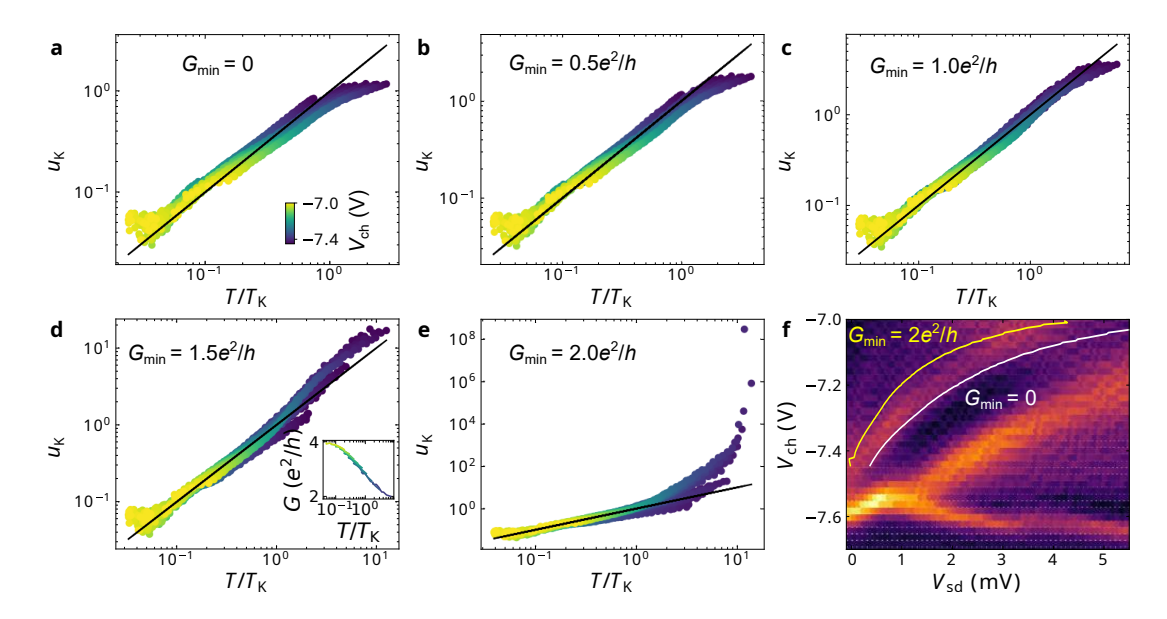


Figure S3. (a)-(e)  $G_{\min}$ -dependence of the universal SU(2) Kondo scaling at different channel gate voltages  $(V_{\text{ch}})$ , indicated by the line colors. The inset of panel d shows the universal scaling of G vs.  $T/T_{\text{K}}$  for  $G_{\min} = 1.4e^2/h$ . (f) Kondo activation bias  $2k_{\text{B}}T_{\text{K}}/e$  obtained for  $G_{\min} = 0$  (white) and  $2e^2/h$  (yellow) compared with the transconductance shown in Fig. S2b.

### S5. TEMPERATURE DEPENDENT TRANSPORT WITH $B_z = 0.6$ T AND FANO PHYSICS

The temperature dependence of the zero-bias G under an out-of-plane magnetic field  $B_z = 0.6$  T is shown in Fig. S4a, where the yellow patch highlights the  $V_{\rm ch}$  range that shows Kondo-like thermal activation (G decreases when increasing T). Figure S4b shows the  $V_{\rm sd}$  dependence, which is also plotted in Fig. 2c of the main manuscript, and the relevant area is marked in yellow to highlight the asymmetric Fano-like ZBP structure. Figure S4c shows the universal Kondo scaling extracted using Equations S1 and S2. Note that the agreement is significantly worse than at  $B_z = 0$ , an expected consequence of the fact that the model only considers Kondo physics, and Fano effects may also influence the T dependence.

To infer whether the bias dependence is indeed consistent with Fano physics, we have fit the  $V_{\rm ch}$  dependence to the Fano formula [76]:

$$G(V_{\rm sd}) = G_0 + c_1 V_{\rm sd} + A \frac{(\epsilon + q)^2}{(1 + \epsilon^2)}$$
 (S3)

where  $G_0$  and  $C_1$  are the background conductance and slope, A is the resonance strength, q is the asymmetry factor,  $\epsilon = (eV_{\rm sd} - E_0)/\Gamma$ , where e is the electron charge,  $E_0$  and  $\Gamma$  are the resonance energy and linewidth. The fits are shown in Fig. S4d as black dashed lines, and the parameters obtained from the fits are shown in Table S1. From these, we conclude that, except for the  $V_{\rm ch} = -7.042$  V case, which has a negative  $\Gamma$  that is likely an artifact of the fit, the remaining traces are consistent with Fano physics. The faint Coulomb diamonds in Fig. S2d, together with the plateau at  $G \approx 0.9 \times 4e^2/h$  in Fig. 3a suggest that variations in the effective QPC width may lead to weakly confined regions when  $B_z$  induces magnetic depopulation [77]. Under such conditions, interference effects consistent with Fano physics [78] provide a plausible explanation for the observed asymmetric ZBPs.

$G_0 (e^2/h) c_1 (e^2/hV)$	$A (e^2/h)$	$E_0 \text{ (eV)}$	Γ (eV)	q	$V_{\rm ch}$ (V)
3.637(24) -137.5(11)	) -0.421(28)	$-1.37(35) \times 10^{-4}$	$1.40(5) \times 10^{-3}$	-1.35(5)	-7.192
3.678(31) -119.6(15)	-0.389(36)	$-2.26(52) \times 10^{-4}$	$1.41(8) \times 10^{-3}$	-1.34(7)	-7.162
3.640(20) -49.4(11)	-0.267(24)	$-3.25(47) \times 10^{-4}$	$1.02(7) \times 10^{-3}$	-1.46(9)	-7.132
3.660(11) -9.46(56)	, ,	, ,	, ,	-2.01(10)	
3.734(8)   4.41(38)	-0.0561(65)	$-7.24(18) \times 10^{-4}$	$5.75(21) \times 10^{-4}$	-3.48(21)	-7.072
3.853(9) $22.91(52)$	-0.0010(14)	$-9.61(26) \times 10^{-4}$	$-5.21(27) \times 10^{-4}$	26.8(186)	-7.042

Table S1. Fano fit parameters reported with uncertainties in a value(uncertainty) format.

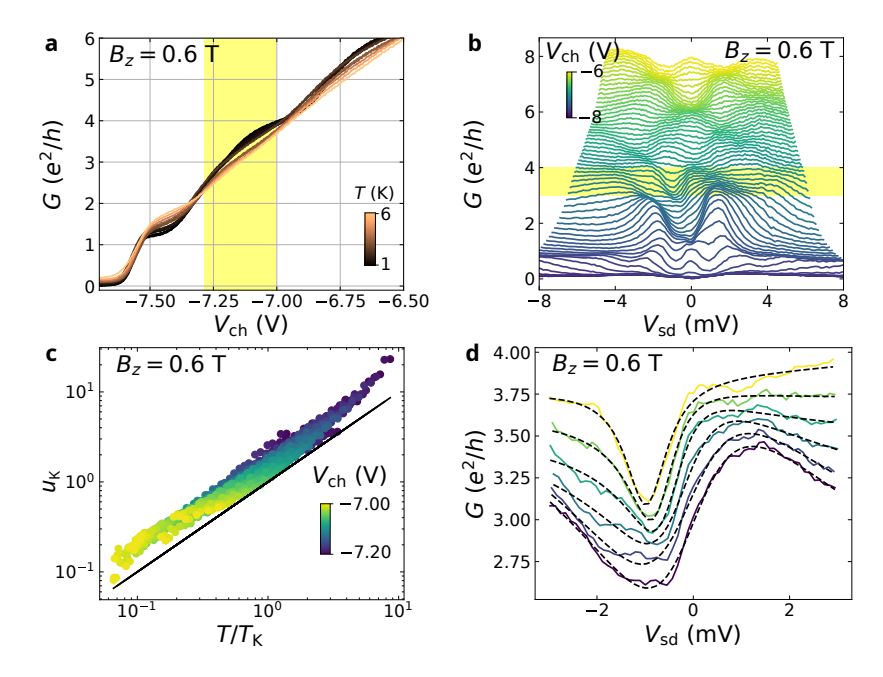


Figure S4. (a) Temperature dependent G vs.  $V_{\rm ch}$ . The yellow patch indicates the area showing the Kondo-like thermal activation. (b) Bias and channel gate dependence with the yellow patch as in a, where the asymmetric Fano-like structure near zero  $V_{\rm sd}$  can be observed. (c) SU(2) Kondo universal scaling with  $G_{\rm min} = 2.5e^2/h$ . (d) Fitting of the low  $V_{\rm sd}$  conductance using Eq. S3. The lines colored according to the colorbar in c are the extracted from panel b. The fits are black dashed lines.

### S6. IN-PLANE MAGNETIC FIELD DEPENDENCE IN A DIFFERENT COOLDOWN

To achieve higher in-plane magnetic field values  $B_{\parallel}$ , we loaded the sample in a cryostat with a base temperature  $T\approx 1.7$  K and  $-8 < B_{\parallel} < 8$  T. The results are shown in Fig. S5 and show the high bias subband at  $G\approx 0.7\times 4e^2/h$  and the ZBP observed in the first cooldown at  $T\approx 1.2$  K, which here has a reduced height. Furthermore, the spin splitting of the  $4e^2/h$  plateau at  $B_{\parallel}=3$  T is also reproduced, and the formation of a well-defined plateau at  $G\approx 2e^2/h$  is observed at  $B_{\parallel}=8$  T. The corresponding transconductance plots are shown in Figs. S5d-S5f.

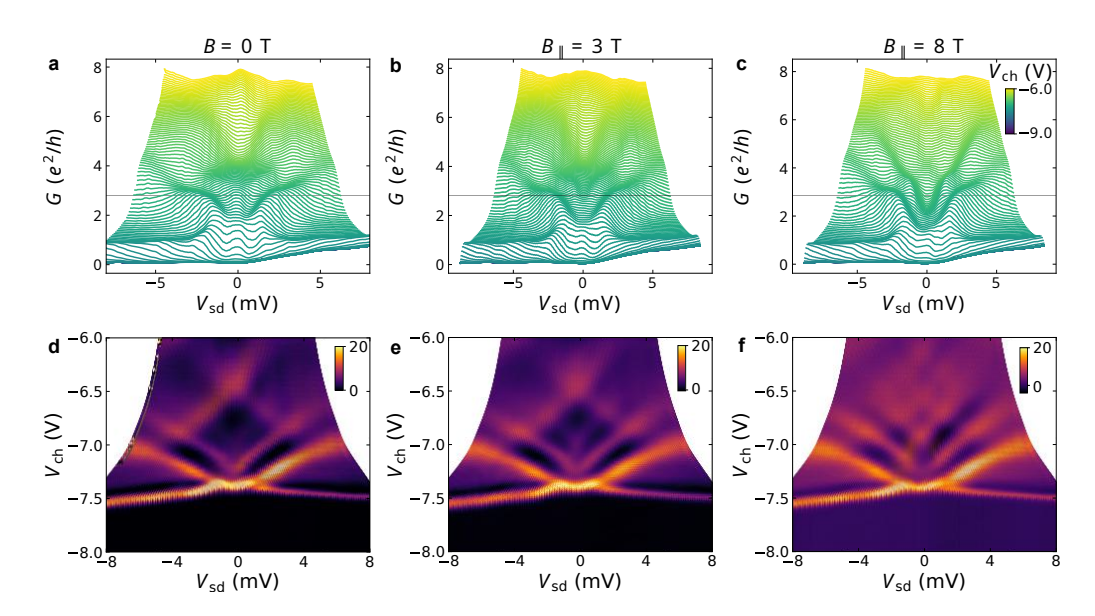


Figure S5. (a)-(c) Evolution of G vs.  $V_{\rm sd}$  at different  $V_{\rm ch}$  with  $B_{\parallel}$  at  $T\approx 1.7$  K and  $V_{\rm bg}=3$  V. The titles indicate the  $B_{\parallel}$  values,  $V_{\rm ch}$  is shown by the line colors, defined by the color bar in panel c, and the horizontal gray lines show  $G=0.7\times 4e^2/h$ . (d)-(f) Transconductance extracted from panels a-c, respectively.

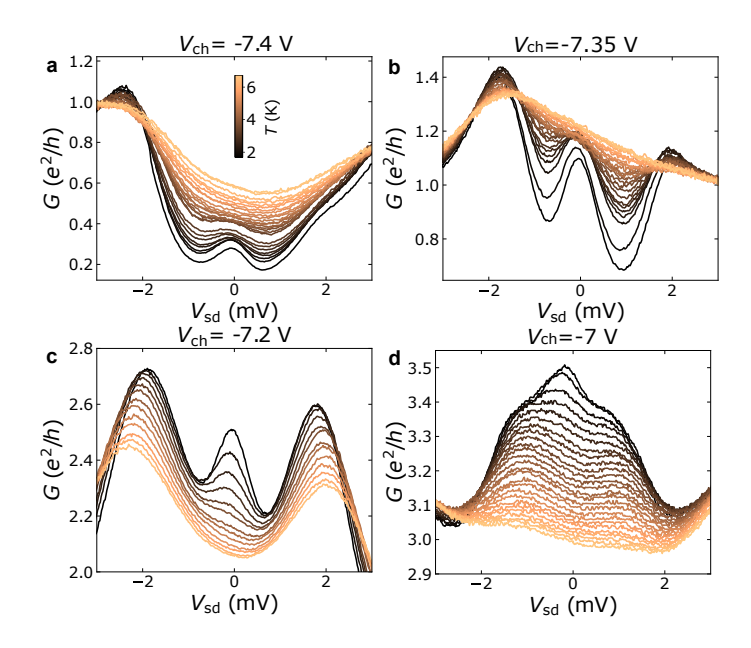


Figure S6. Zero bias peak evolution with temperature at  $V_{\rm ch} = -7.4$  (a),  $V_{\rm ch} = -7.35$  (b),  $V_{\rm ch} = -7.2$  (c), and  $V_{\rm ch} = -7$  V (d). The line color, specified by the color bar in panel a, shows the temperature T. These results were obtained during the second cooldown at B = 0 and  $T \approx 1.7$  K.

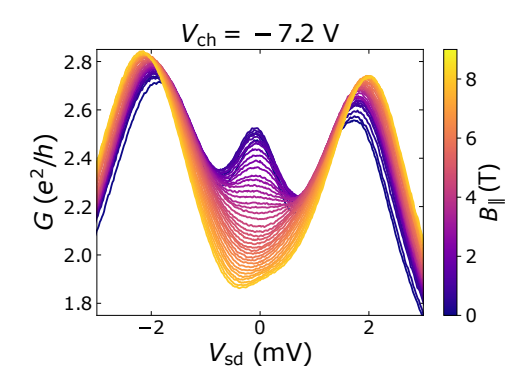


Figure S7. In-plane magnetic field dependence of the zero bias peak at  $T \approx 1.7$  K and  $V_{\rm ch} = -7.2$  V. These results were obtained during the second cooldown at  $T \approx 1.7$  K.

### S7. TEMPERATURE DEPENDENCE OF ZERO-BIAS PEAK

The T evolution of the ZBPs is shown in Fig. S6 for different  $V_{\rm ch}$  and shows that, for  $V_{\rm ch} \leq -7.2$  V, the peak disappears when heating. In contrast, for  $V_{\rm ch} = -7$  V, instead of a single peak, two peaks are observed at 1.7 K. When heating, a single peak arises near  $V_{\rm sd} = 0$ . We attribute these behaviors to the complex T dependence shown by the 0.7 anomaly in QPCs [26]. Note that, for  $V_{\rm ch} < -7.2$  V, the zero bias G increases with T, indicating a thermally activated current path, most likely under the split gates due to the small gap.

### S8. MAGNETIC FIELD DEPENDENCE OF ZERO-BIAS PEAK

The in-plane magnetic field dependence of the ZBP measured at  $V_{\rm ch} = -7.2$  V is shown in Fig. S7. In contrast with Fig. 3 in the main manuscript, the zero bias peak does not split into two when increasing  $B_{\parallel}$  and instead turns into a minimum. This behavior has been observed at other  $V_{\rm ch}$  in Fig. 3 of the main manuscript and in previous QPC works in 2DEG systems, such as Refs. [16, 26].

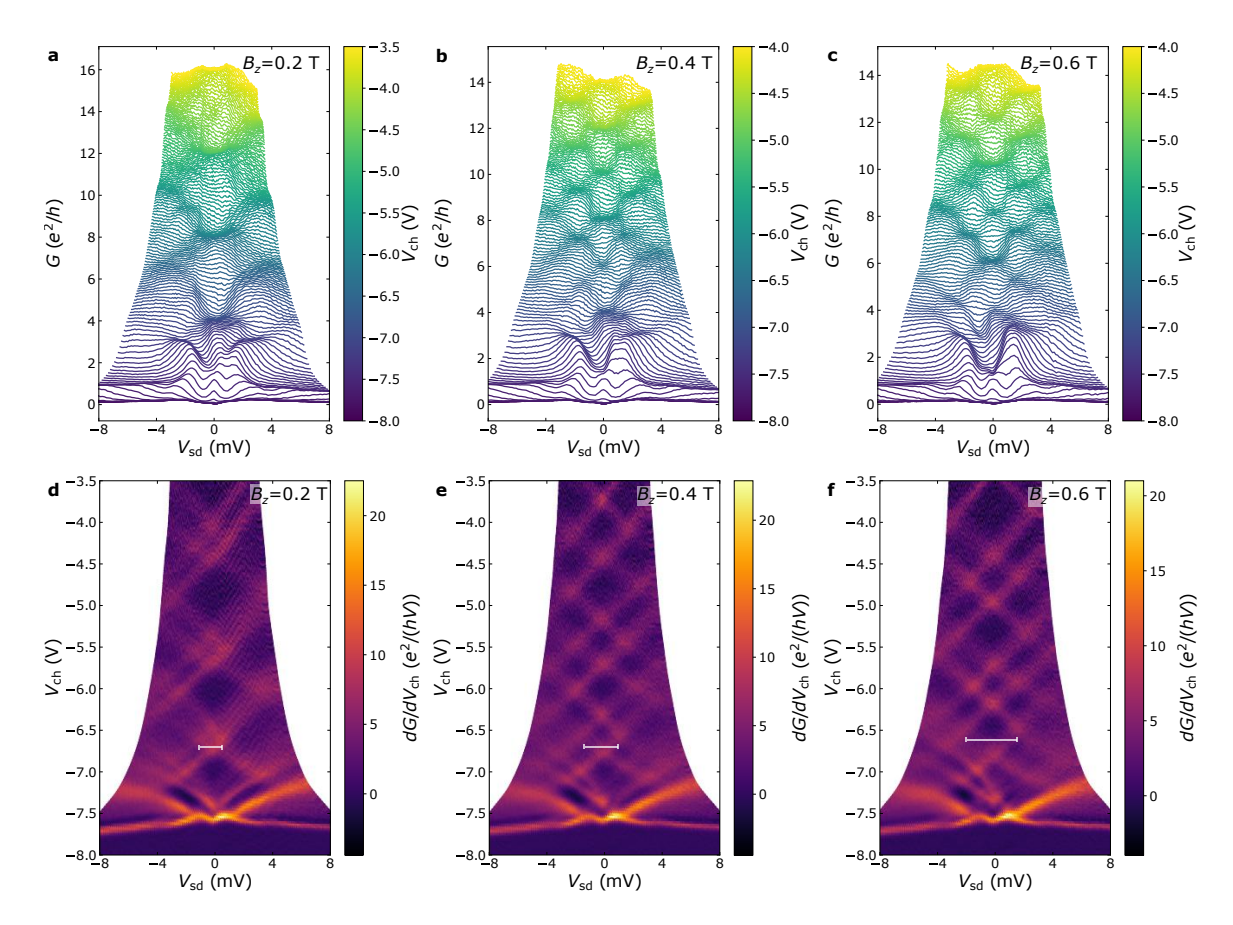


Figure S8. Effect of an out-of-plane magnetic field on the  $V_{\rm sd}$  and  $V_{\rm ch}$  dependence of the QPC conductance. (a-c) QPC conductance vs.  $V_{\rm sd}$  at different  $V_{\rm ch}$  values for  $B_z=0.2,\,0.4,\,$  and 0.6 T, respectively. (d-f) QPC transconductance vs.  $V_{\rm sd}$  and  $V_{\rm ch}$  for  $B_z=0.2,\,0.4,\,$  and 0.6 T, respectively. The white horizontal lines indicate the  $B_z$ -induced second subband splitting.

### S9. DETERMINATION OF THE VALLEY g FACTOR

It has been shown that BLG QPCs respond to an out-of-plane magnetic field  $B_z$  with a valley splitting [50–52]. The energy splitting is proportional to the applied  $B_z$  and follows  $\Delta E_Z = g_v \mu_B B_z$ , where  $g_v$  is the valley g factor and  $\mu_B$  is the Bohr magneton. Since  $g_v$  depends on the QPC width [71], we have measured the effect of  $B_z$  on the QPC conductance and transconductance to determine  $g_v$ . The results are shown in Fig. S8. In panels a-c, the G traces are shown vs.  $V_{\rm sd}$  and for different  $V_{\rm ch}$ , demonstrating the breaking of the subband degeneracy from 4 down to 2, due to the valley splitting. Figure S8d-f shows the QPC transconductance, which we used to extract the valley splitting  $\Delta E_z$ . The white horizontal lines show  $2\Delta E_z/e$  for the  $G=2\times 4e^2/h$  subband. The  $\Delta E_z$  values have been collected and plotted vs.  $B_z$  in Fig. S9 where linear fits to  $\Delta E_Z = g_v \mu_B B_z$  have been used to extract the  $g_v$  for the G=8, 12, and  $16\times e^2/h$  subbands.

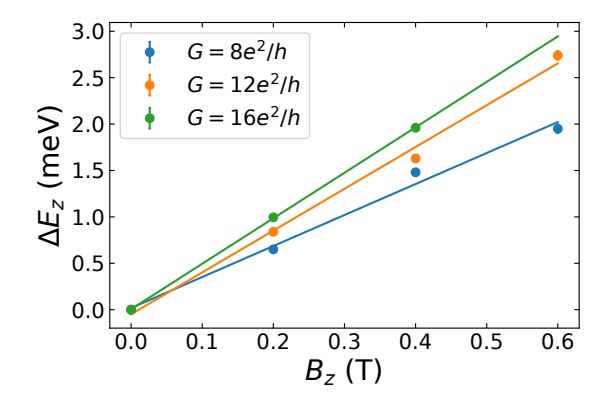


Figure S9.  $B_z$ -induced subband splitting ( $\Delta E_z$ ) obtained from Fig. S8 for the first three subbands (scatter). The lines are fits to  $\Delta E_Z = g_v \mu_B B_z$ , resulting in  $g_v = 58 \pm 4$ ,  $78 \pm 4$ , and  $85 \pm 1$  for the G = 8, 12, and  $16 \times e^2/h$  subbands, respectively.